Terasense WP03 Radiation and Sensor Measurement Lab Workpackage

Y. Álvarez López[(1)], S. Burgos[(2)], F. Cano Fácila[(2)], Pedro García-del-Pino[(3)], F. Las Heras Andrés[(1)], J. Laviada Martínez[(1)], A. Muñoz-Acevedo [(2)], José M. Riera[(2)], M. Sierra-Castañer[(2)], M. Sierra-Pérez[(2)], Gustavo A. Siles[(2)]

yalopez@tsc.uniovi.es, sara.burgos@upm.es, francisco@gr.ssr.upm.es, pedro.gdelpino@upm.es, flasheras@tsc.uniovi.es, jlaviada@tsc.uniovi.es, alfonso@gr.ssr.upm.es, jm.riera@upm.es, manuel.sierra@upm.es, m.sierra.perez@gr.ssr.upm.es, gsiles@grc.ssr.upm.es

(1) Dpto. De Teoría de Señal y Comunicaciones, Universidad de Oviedo, Campus de Viesques, Gijón, Asturias, Spain.

(2) Dpto. de Señales, Sistemas y Radiocomunicaciones, Universidad Politécnica de Madrid ETSI de Telecomunicación, Ciudad Universitaria s/n, 28040, Madrid, Spain.

(3) Dpto. de Ingeniería Audiovisual y Comunicaciones, Universidad Politécnica de Madrid EUIT de Telecomunicación, UPM Campus Sur, Cta. de Valencia, km 7, 28031, Madrid, Spain.

***Abstract*- This paper explains the progress accomplished in the WP03 of the Terasense Project (TERAHERTZ TECHNOLOGY FOR ELECTROMAGNETIC SENSING APPLICATIONS) approved in the 2008 CONSOLIDER-INGENIO program (project CSD2008-0068). The Radiation and Sensor Measurement Lab (RSMLab) is a laboratory based in the existing antenna measurement laboratories at UPM, UC3 and UNiOvi and the new capacities to extend the measurement range from the millimetre wave to the THz region. This laboratory is intended to be shared in more than one place and with more than one institution, in such a way that we could take advantage of other research financial sources and contributions from other institutions with interest in the same field of measurements. One important task will be the international links between the RSMLab and other European and international institutions dedicated to the antenna and sensor measurement in the same frequency range.**

I. INTRODUCTION: CONTEXT AND OBJECTIVES

The main objectives proposed in this WP are:

- Creation of the Laboratory. Study of existing capacities and design of new needs to extend the measurement frequency range and measurement methods.
- Definition of three benches to hold the measurement needs in the three prototypes included in the Consolider Project: 90 GHz Short Range Cámera, 300 GHz Remote Sensor and 1.1 THz Bio Spectrometer.
- Study of synergy between RSMLab and other institutions and research projects to avoid redundancy and support the high budget needed to build this laboratory. It will be considered the collaboration with National Research Projects from the Research Ministry, from the local communities (Madrid, Asturias etc.), from European projects (FP7) and from institutions (Universities, CSIC, etc)
- Design and construction of the three measurement benches in the mm and THz frequency bands. These three benches can be placed in the same physical place or shared between two or more places, depending on the capacities, budget possibilities and measurement needs. In fact, the frequency is not the most important parameter to separate the three benches but the prototype working mode and measured parameters.
- Integration in the European Antenna Measurement Network depending on the European Association on Antennas and Propagation of waves (EurAAP). Collaboration with other antenna and source measurement labs in the THz region.
- Integration in the Standard Definition and Discussion Groups. It is very important to be included in the committees dedicated to develop and define measurement standards in these new developed measurement systems.

These objectives were planned in three tasks. The objective of first one, THz Antenna Measurement System, is the design and construction of an antenna measurement system to obtain information of antenna pattern, input impedance, gain and other antenna parameters in the millimeter and THz bands. The design of these antenna measurement benches is an important task that must be followed by the construction with the adequate equipment. The capacity of rising in frequency and antenna dimensions depends mainly on the budget for this task, either coming from this project of from other founding contributions.

The second task deals with Holographic Diagnostic and Imaging. Large antenna measurement in the frequency range from 90 GHz to 1 THz require large anechoic cameras or field phase measurements that are very difficult to obtain with high accuracy in these bands. This task propose amplitude only measurement with an amplitude transformation from near to far field region to give capacity for large antenna measurement in conventional chambers.

The third task is related to THz Propagation Characterization. This task studies the THz wave propagation in atmospheric gases and clouds, including prediction and

measurement techniques, and propagation under the presence of hydrometeors.

The structure of the paper has followed the three tasks: the second section deals with the setup implementation, the third section with the algorithms to improve some aspects in the antenna measurement results at these frequencies, and the fourth section with the propagation aspects. Finally, the last section summarizes the main conclusions and results obtained through the period of this project.

II. THz Antenna Measurement System

This task has been focused on two aspects: first the HW implementation. Different setups in 75-110 GHz and 220-325 GHz have been designed for antenna measurement. The first one is being used for the measurement of one of the arrays antennas in the Project. Also, new technique for the design of Compact Antenna Test Range has been applied at millimeter and submillimeter ranges.

A. Antenna Measurement Setup at 100 and 300 GHz

A first study analyzing the advantages and disadvantages of the different antenna measurement setups at those frequency bands (specially 300 GHz) were developed [1] and [2]. The main results are summarized in Table 1.

	Far field	**PNF**	**CATR**	**Hologram**
Antenna size	Small	Large	Medium	Medium
Frequency band	Large	Large	Large	Small
Dynamic Range	Short measurement distance	Good	Short focal distance	Good
Accuracy	Good	Fair-due to phase measurements	Good	Average
Complexity	Low	High	High	Medium
Experience of the team	Yes	Yes	Yes	No

Table 1: Summary of antenna measurement technologies at 300 GHz.

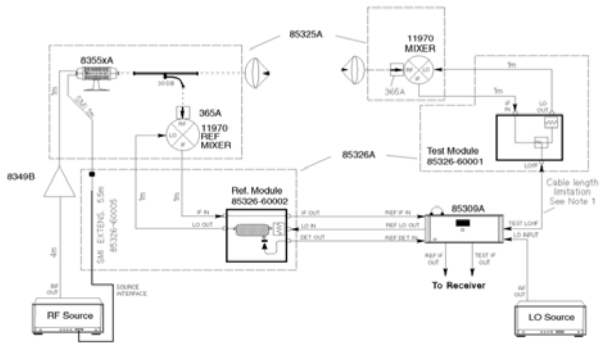

Fig. 1. Antenna Measurement setup at 100 GHz

In any case, the RF equipment at these frequency bands were the conventional ones. The 75-110 and 220-325 GHz setups are based on commercial mixers, multipliers and amplifiers. Figure 1 shows the 100 GHz setup. This setup has been used for measurement of the stability of field with variations of temperature and humidity at these frequency bands and now it is going to be used for measuring one of the antennas designed for this project. The instrumentation for the 220-325 GHz setup will be ready in few months.

B. Algorithm for the design of Compact Antenna Test Ranges at mm and sub-mm frequencies.

A method to analyze parabolic reflectors with arbitrary piecewise rim is presented in this paper [3]. This kind of reflectors, when operating as collimators in compact range facilities, needs to be large in terms of wavelength. Their analysis is very inefficient, when it is carried out with fullwave/MoM techniques, and it is not very appropriate for designing with PO techniques. Also, fast GO formulations do not offer enough accuracy to reach performance results. The proposed algorithm is based on a GO-PWS hybrid scheme, using analytical as well as non-analytical formulations. On one side, an analytical treatment of the polygonal rim reflectors is carried out. On the other side, non-analytical calculi are based on efficient operations, such as M^2 order 2-dimensional FFT. A combination of these two techniques in the algorithm ensures real ad-hoc design capabilities, reached through analysis speedup. The purpose of the algorithm is to obtain an optimal conformal serrated-edge reflector design through the analysis of the field quality within the quiet zone that it is able to generate in its forward half space. The problem is shown in Fig. 2

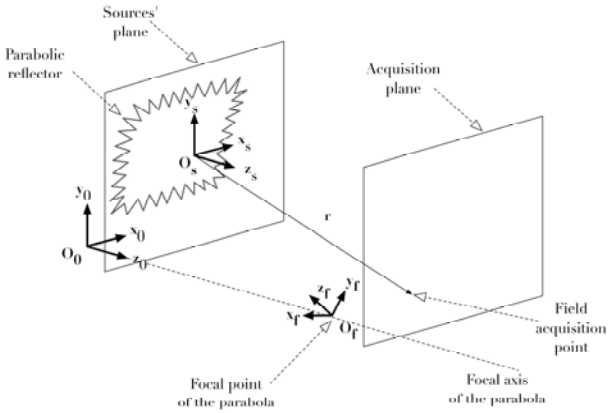

Fig. 2. Analysis Model

Our purpose is to obtain plane acquisitions of electric field inside the Fresnel region of a serrated-edge reflector. Thus, the results to be studied will be E/H-plane cuts of the diffracted electric field, in a compact-range, where the feeder is pointing to the center of the reflector. The obtained results are compared to electric field results from GRASP8, that is the reflector analysis tool more widely used to carry out PO analysis over reflector antennas.

A circular offset reflector with linear serrated edge has been studied. The setup definition is presented in table II. This reflector has a high F/D, which minimizes the amplitude slope in the vertical cut; 36 test serrations of 0.1 m length are placed around a circular rim with 0.2 m of radius. The feeder follows a Gaussian pattern, with -1 dB at θ=10º and non ϕ–dependent. Amplitude and phase cuts are shown in Fig. 4 and 5. A good agreement is observed for both magnitudes in the vertical cut, whereas horizontal acquisition has not the same level of agreement. The analysis performed using MoM, observes similar discrepancies between PO and MoM. In any

case, this hybrid method can give accurate results to bound the ripple and the tapering in a single reflector CATR for these frequency bands. After simulation results have been shown, speedup notes must be added to offer a clear idea of the algorithm's global performance. Simulation times are considered, as overall indicators. The algorithm has been implemented in FORTRAN code, and uses high performance FFT external modules. Simulations were carried out in a 2.8 GHz double core Pentium 4 processor, with 4 GB of RAM. GRASP8 took 31.500s to reach the results. On the other side, the implementation of the algorithm took 11s to reach its results.

TABLE II
TEST REFLECTOR B: SERRATED CIRCULAR REFLECTOR SIMULATION

Parameter	Value
Frequency	100 GHz
D	0.6 m Internal radius: 0.2 m Serration depth: 0.1 m
Doffset	0.2 m
focal distance	2.5 m
zshift	3.0 m
zoffset	0.128 m
Feed pattern	Gaussian: -1.0 dB for θ=10º.

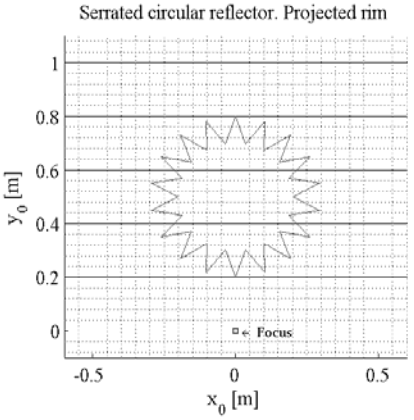

Fig. 3. Serrated reflector projected rim

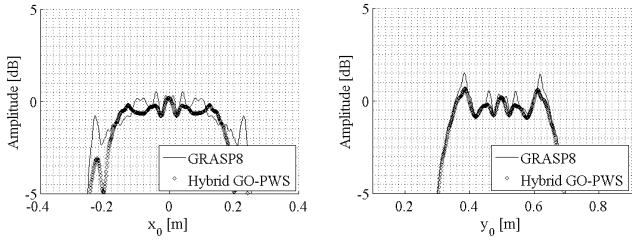

Fig. 4. Normalized amplitude, horizontal and vertical cuts; serrated reflector

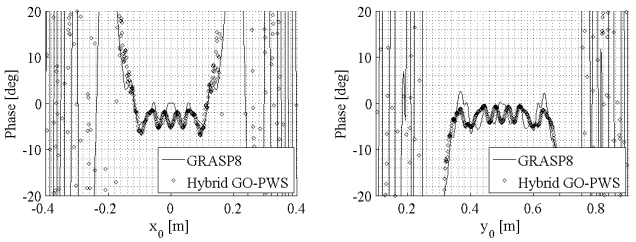

Fig. 5. Normalized phase, horizontal and vertical cuts; serrated reflector

III. HOLOGRAPHIC DIAGNOSTIC AND IMAGING

The research under this topic has been divided in two areas:

- Source reconstruction techniques for the antenna diagnostic and holography.
- Algorithms for the improvement of the results in the antenna Measurement systems at mm and sub-mm frequency bands.

A. Source reconstruction techniques for the antenna diagnostic and holography

Algorithms and measurement setups for imaging measurements using amplitude and phase information have been previously reported in the 90GHz [9] and in the 240GHz band [10]. Some experiments approaching THz band are in progress, but any approach requiring phase information at sub-mm and THz frequency bands requires expensive equipment due to the need of accurate phase acquisition. Even with state of the art instrumentation, it could be difficult to get the necessary accuracy (in antenna and imaging applications) if a direct phase acquisition at such frequencies is conducted.

In the last decades, several phase retrieval methods have been proposed: on the one hand, those that recovers phase information from the measured field amplitude in two or more acquisition planes [4],[5]; on the other hand, those based on combining the measured field with a known reference field [6],[7]. The latter techniques are usually referred to as Leith-Upatnieks holography.

The setup described in this section combines the measured field with a sample of the source signal that has been conveniently attenuated and phase shifted to emulate a certain reference wave (e.g., a plane wave). Moreover, reference signal phase shifting is achieved by displacing the probe antenna (see Fig. 6), thus avoiding the need of a phase shifter, which can be expensive at sub-mm and THz frequency bands. After phase information is retrieved, general purposed algorithms for antenna diagnosis can be applied [8].

To prove the validity of the phaseless setup for antenna diagnostics, an application example is shown: the antenna-under-test (AUT), a horn antenna, is distorted by covering part of the aperture with aluminum foil. First, the complex radiated field at the working frequency of 15 GHz is acquired using a Vector Network Analyzer (VNA). The plane wave spectrum is represented in Fig. 7, clearly showing the differences between non-distorted and distorted AUT radiated fields.

Focusing on the distorted case, the measured field using the proposed phaseless setup is acquired. Once the phase is retrieved, the field is backpropagated to the aperture plane [8] in order to analyze aperture field distribution, as shown in Fig. 8 (a),(c): the aperture blockage yields a field level reduction (upper side of the aperture in Fig. 8 (a)).

Next, differences between aperture fields using measured and retrieved phase are evaluated. Amplitude and phase differences are plotted in Fig. 8 (b) and (d), respectively: amplitude differences are less than 5 dB within the aperture area, whereas phase error is 15 degrees at most, thus confirming the suitability of this setup for phaseless antenna diagnostics.

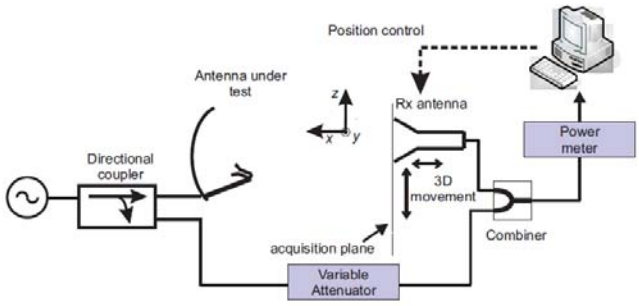

Fig. 6. Proposed setup for phaseless measurements.

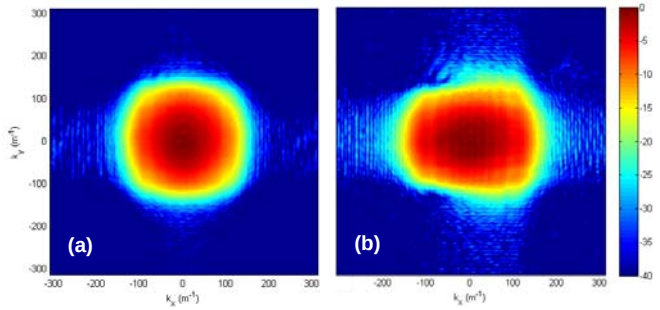

Fig. 7. Plane wave spectrum amplitude (in dB) of the measured field. Horn antenna without distortion (a) and with aluminum foil blocking part of the aperture (b).

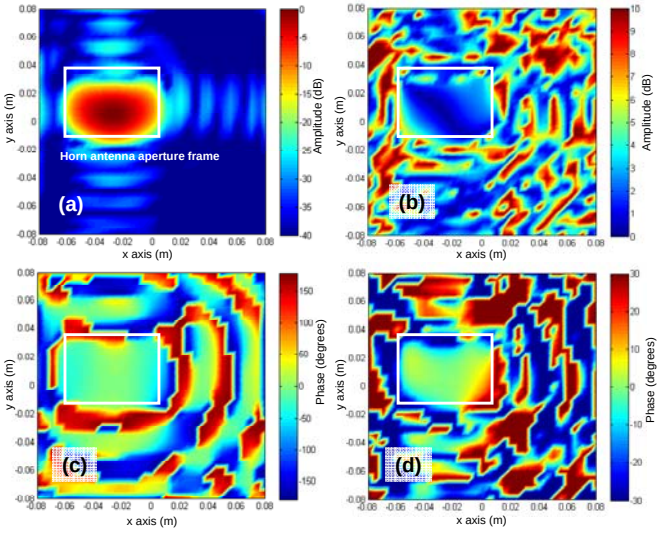

Fig. 8. Reconstructed electric field (amplitude (a) and phase (c)) on the distorted horn antenna aperture plane using measured amplitude and retrieved phase. Differences (in amplitude (b) and phase (d)) between reconstructed aperture fields using measured and retrieved phase data.

B. Algorithms for the improvement of the results in the antenna Measurement systems at mm and sub-mm frequency bands.

The sources reconstruction technique can be employed to detect errors, and also identify which are the causes of such errors [11-16], for example, electrical errors in arrays or mechanical errors in reflectors. Apart from its classic application, a diagnostic process also gives a complete electromagnetic characterization of the antenna, which is the basis of other applications, like near- to far-field transformations, radome applications, radioelectric coverage, etc. In this work, that additional information is employed to reduce the effect of common errors in antenna measurements. This technique has been used for the next applications:

Reflection suppression method

Normally, the antenna measurements are carried out in anechoic chambers to reduce unwanted contributions, such as reflections or diffractions from the environment. However, there are special cases in which the use of that kind of measurement setup is not possible, and a semi-anechoic chamber or an outdoor measurement system has to be employed. In fact, reflection waves may also appear in anechoic chambers due to imperfections in the radiation absorbing material (RAM). In any case, when the measurement is not performed in a fully anechoic environment, the unwanted contributions could significantly alter the actual antenna properties, producing a ripple in the radiation pattern.

The proposed method is based on a diagnostic technique. The input data are taken over only one arbitrary surface in the frequency-domain. Moreover, compared with some time-gating techniques or frequency decomposition techniques, it is not necessary to measure more than one frequency. Therefore, the measurement time is reduced considerably and, because the frequency-domain is employed, complicated equipment is not needed. If reflected waves are present in antenna measurements, the radiation properties obtained will be perturbed. These same incorrect results are achieved with an equivalent system where reflections can be viewed as direct waves coming from virtual sources, as shown in Fig. 9. Such a replacement is explained in detail via image theory. The identification of the virtual sources is not possible with a conventional diagnostic technique, where the field is only reconstructed over the antenna aperture. However, if the field reconstruction is performed over a surface larger than the antenna dimensions, the aforementioned fictitious sources can be found and cancelled with a filtering process.

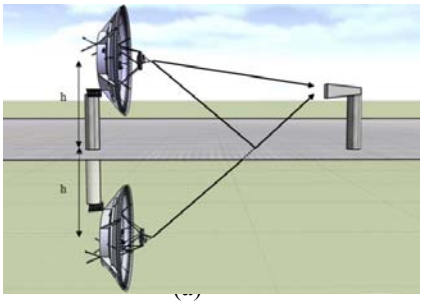

Fig. 9. Reflections in antenna measurements viewed by means of image theory.

By applying any of the reconstruction methods explained before, the extended reconstructed field can be found. In the reconstructed domain, real sources and virtual sources are not spatially coincident. Therefore, a spatial filtering can be applied to suppress those virtual sources associated to the reflections. This filtering is defined as follows

$$F_1(x,y)=\begin{cases}1 & \forall\ (x,y)\notin Z_V\\ 0 & \forall\ (x,y)\in Z_V\end{cases} \quad (1)$$

where Z_V represents the zone where virtual sources are placed. Regardless of the method choice, after the diagnostic stage, the field distribution over the extended AUT plane is

known, and virtual sources can be identified. Then, these sources are filtered out by employing the spatial filtering defined in (1). Finally, a new corrected PWS is obtained by taking the inverse Fourier transform of this filtered field distribution.

To verify the accuracy of the presented method, a measurement using the planar near-field range in the antenna test facility of the Technical University of Madrid (UPM) was performed. For the experiment, the probe and the AUT were selected to be a corrugated conical-horn antenna and a pyramidal-horn antenna, respectively, and they were separated from each other by 1.57 m. A reference measurement over a 2.4 m × 2.4 m acquisition plane was recorded in order to have a pattern with which to compare the future results with reflections and reflection suppression. Then, a rectangular metallic plate was placed in the anechoic chamber, as see in Fig. 10, so as to introduce reflections in the measurement with the AUT at a height of 1.3 m above the plate. Fig. 11 shows a comparison with the reference far-field, where it is possible to see a large ripple in the upper lateral lobe as a consequence of the disturbance generated by the reflective surface. After the reflection suppression, the estimated radiation pattern was obtained, which shows a very good agreement with the reference pattern, as observed in Fig. 11.

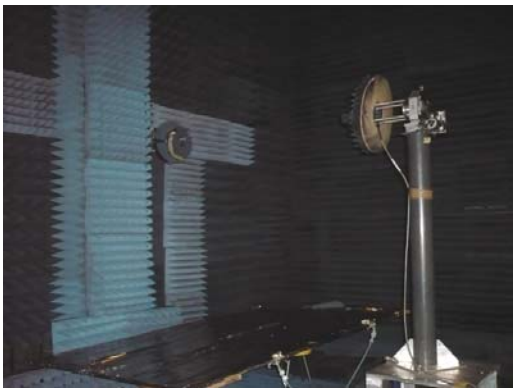

Fig. 10. Experimental setup with a metallic plate.

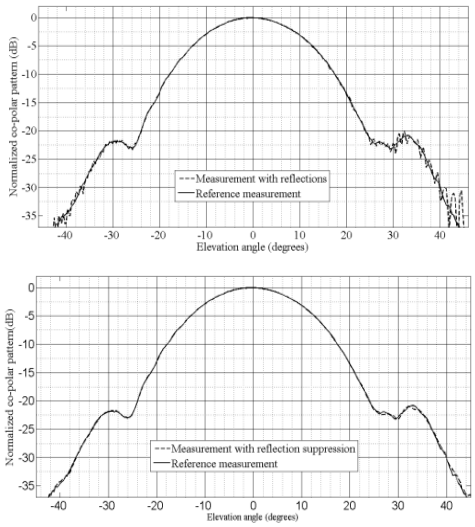

Fig. 11. Comparison between the reference pattern and the pattern with reflections and with reflection suppression technique for the φ=90º.

Noise suppression method

Random noise is one of the errors that limit the accuracy of far-field results, particularly, when measuring a low-sidelobe or a high-performance antenna. One possible source for this error is receiver noise that is present in all measurements. Some comprehensive studies for random noise in near-field measurements have already been presented [14]. The second method proposed in this section is also based on diagnostic techniques and tries to increase the signal-to-noise ratio in the far-field pattern obtained from a planar near-field measurement by reducing the noise power. In the proposed algorithm, once the planar near-field measurement has been performed, the field at the AUT plane (reconstructed field) is computed. Because, the desired contribution is theoretically located inside the dimensions of the AUT, filtering can be applied to cancel the outside contribution due to noise. An analysis to assess the noise behavior and to obtain its statistical parameters was carried out. In the analysis, a complex white Gaussian and space-stationary zero mean noise was considered. From this analysis, it was deduced that, for planar near-field noise with the aforementioned statistical characteristics, the noise in the reconstructed field is a complex, stationary, white Gaussian noise, with zero mean and a variance that is equal to the variance of the noise in the scan plane. Because the noise is kept stationary, i.e., the noise power is identically distributed on the reconstructed surface, and the desired contribution is theoretically concentrated in the region where the AUT is located, a filtering can be applied to cancel the noise out of the AUT dimensions. The definition of filtering appears in (2).

$$F_2(x,y)=\begin{cases}1 & (x,y)\in \omega_{\mathrm{A}} \\ 0 & (x,y)\in \omega_{\mathrm{T}}-\omega_{\mathrm{A}}\end{cases} \tag{2}$$

where w_T and w_A represent the reconstructed region and the AUT region. Because the noise is identically distributed over the reconstructed surface, the signal-to-noise ratio improvement achieved with the proposed spatial filtering method is the ratio between the surfaces of both reconstructed regions (3).

$$\Delta SNR=\frac{S_{\omega_T}}{S_{\omega_A}} \tag{3}$$

First, the measured data are used to obtain the PWS, referenced to the scan plane, by using an inverse Fourier transform (IFT). The next steps are to reference the PWS to the AUT plane and to calculate the reconstructed field. Then, noise filtering can be used. Finally, a new PWS with less noise power is computed using again an IFT. The validation of this method was carried out by employing the data of the reference measurement presented in the previous method. Gaussian noise with 30 dB less power than the maximum of the acquired data was computationally added. The noise power was chosen to be large so as to ensure a negligible measurement noise. Thus, the far-field obtained from the measured data without additive noise can be used as a reference to compare results before and after noise filtering. The results both for the co-polar and cross-polar pattern are shown in Fig. 12. In this particular case, the improvement calculated as indicated in (3) was equal to 28.27 dB.

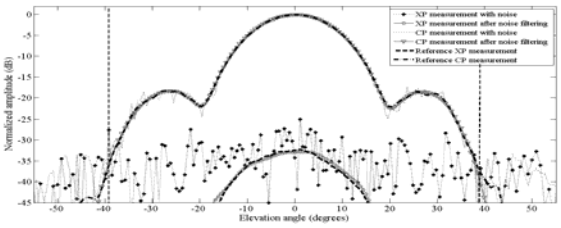

Fig. 12. Comparison between the reference pattern, the pattern with noise and the pattern after the noise filtering in ϕ = 90º plane. The boundaries of the reliable region are indicated by vertical dotted lines.

Techniques to improve the quality of the quiet zone in compact ranges

Other algorithms have been used for improving the quality and reducing the measurement time in CATR at mm and sub-mm frequencies [16]. CATR measurement facilities are characterised by a straightforward operation which is able to perform real time antenna measurements along a wide margin of frequencies, whenever reflectors or lenses are used as collimators. In spite of their compactness, CATR facilities operate in far-field conditions. Therefore, the test wave received by the AUT should be a plane wave. The operation of a CATR relies on the planarity of this test wave, inside the "quiet zone" volume. Electromagnetic theory states that the quiet zone region cannot hold a plane wave field distribution, even not with an arbitrarily small volume, for a finite frequency of operation. This is due to the ability of the range's collimator to concentrate the electromagnetic energy within a reduced set of angular directions, following a distribution which is expected to tend to the delta in the angular domain when moving up in frequency. Long term stability of this planarity is achieved through temperature and humidity control inside the chamber and surrounding the instrumentation. The performance of the facility is maximized if these magnitudes are sampled and used as feedback to perform field correction. An ambience sensor samples atmospheric pressure (P), relative humidity (RH) and temperature (T). The environmental model of field propagation uses these magnitudes as inputs and corrects the phase ($\Delta\varphi$) of the probed field taking into account the variation of the air's refractive index *n(T,P,RH)*, as in Eqs. (4 and 5). Pressure is measured in *hPa*, T is measured in *K* and Δr states for the path length from the feed towards the test zone, in meters. Coefficients *a*, *b*, *c* can be found in the ITU P.453-9 recommendation.

$$\Delta\phi\left(T,P,RH\right)=\frac{2\pi}{\lambda_0}\cdot n\left(T,P,RH\right)\cdot\Delta r \qquad (4)$$

$$n\left(T,P,RH\right)=1+\frac{77.6}{T}\cdot\left(P+4810\cdot\frac{1}{T}\cdot\frac{RH}{100}\cdot a\cdot\exp\left(\frac{b\cdot\left(T-T_0\right)}{\left(T-T_0\right)+c}\right)\right)\cdot10^{-6} \qquad (5)$$

Developments on the Assessment of Compact Antenna Test Ranges at Millimeter Wavelengths

Quiet zone sampling is a powerful tool to understand the behavior of a CATR's performance. However, at mm and submm frequencies the acquisition time can be prohibitive. When the test zone field distribution is known for N_{RF} frequencies within a certain RF bandwidth, diverse post-processing techniques can be performed, such as time-gating.

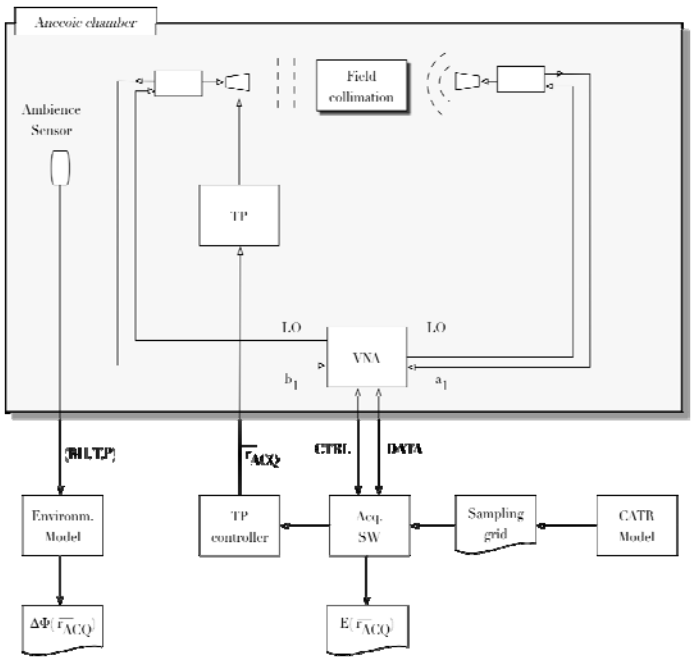

Fig. 13. CATR quiet zone data acquisition setup.

In our case of interest, time gating is needed and it is used to isolate the direct ray contribution, arriving from the main reflector. In addition, low IFBW is required to ensure weak levels of noise with respect to the signal, which is already expected to be low.

The plane wave's spectral $\widetilde{\Omega}_0=\left[-k_0,k_0\right]\times\left[-k_0,k_0\right]$ includes visible angles within a radiation hemisphere centered in the sources and directed towards the downrange direction, in addition with some cutoff non-radiating modes. However, the coupling between the sources, within Ω_S, and the quiet zone acquisition domain $\boldsymbol{\Omega}_A=\left[x_A^-,x_A^+\right]\times\left[y_A^-,y_A^+\right]$ occurs through a reduced compact set of spectral modes within the spectral domain $\widetilde{\Omega}_{Range}\subset\widetilde{\Omega}_0$, deduced in (6) .

$$\widetilde{\Omega}_{Range}=\left[-k_{x,Range},k_{x,Range}\right]\times\left[-k_{y,Range},k_{y,Range}\right] \qquad (6)$$

The maximum components reachable by k_x and k_y are $k_{x,Range}$ and $k_{y,Range}$, respectively. They are analytically deduced in Eqs. (7, 8) from a geometrical approach that evaluates the maximum coupling angles $\theta_{C,\{x/y\}}$ based on the geometry of the system. No signal is expected on $\widetilde{\mathbf{E}}\left(\mathrm{k_x},\mathrm{k_y}\right)$ when the spectral components $\left(k_x,k_y\right)\notin\widetilde{\Omega}_{Range}$.

$$k_{x,Range}=k_0\cdot\sin\left(\theta_{C,x}\right)\le k_0 \qquad (7)$$

$$k_{y,Range}=k_0\cdot\sin\left(\theta_{C,y}\right)\le k_0 \qquad (8)$$

Therefore, an undersampling can be applied for the quiet zone assessment of the CATR in the same sense that it is applied in the planar near field measurements. This technique was validated in ESA-ESTEC CATR up to 200 GHz with accurate results in amplitude and phase (Fig. 14).

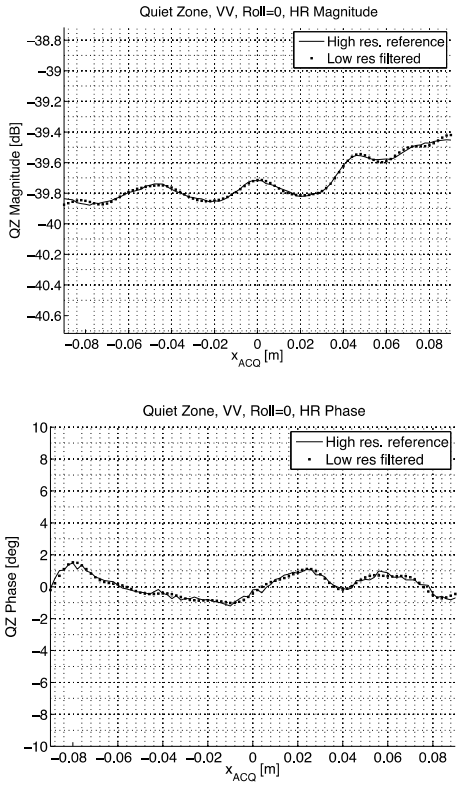

Fig. 14. Sampling performance at 48 GHz. (a) Co-polar acquisition: magnitude, (b) phase.

IV. THz PROPAGATION CHARACTERIZATION

A. *Fundamentals*

Atmospheric propagation at mm (30-300 GHz) and sub-mm (300 GHz-3 THz) ranges is mainly affected by the influence of tropospheric constituents, including atmospheric gases, suspended liquid water droplets, i.e. clouds, and precipitating hydrometeors. Between the gaseous constituents, water vapor exhibit the most important absorption characteristics due to the joint effect of its individual resonance lines (22.23, 183.3 and 325.5 GHz) in combination with a water vapor continuum extending along the entire frequency range. Molecular oxygen has a reduced effect out of its 50-70 GHz attenuation band and its resonance line at 118.7 GHz.

According to the theory of radiation-particle interaction describing the basis of cloud attenuation effects, under Rayleigh regime, whose validity up to 300 GHz have been discussed in [17], scattering caused by cloud liquid water droplets can be considered negligible. Therefore, resulting extinction phenomena have a straight relation with absorption processes within the cloud and linearly related to its liquid water content.

Finally, an accurate approach to estimate extinction caused by rain, due to the combination of absorption and scattering effects, is highly dependent on the drop size distribution during the precipitation [18].

B. *Radiosonde data for atmospheric attenuation prediction*

Under non-rainy conditions, attenuation caused by water vapor and liquid water are of primary interest. A first step in order to quantify both impairments consists on an adequate description of the propagation medium, in terms of its physical parameters. With this purpose, a suitable sensing technique is the use of radiosonde observations (RAOBs), allowing vertical distribution of temperature, atmospheric pressure and relative humidity to be acquired. Therefore, both physical and empirical predicition models have to be used in order to calculte the attenuation contribution of atmospheric gases [20-21] and clouds [22] along a path, using meteorological parameters as input data. An exhaustive analysis of a 5-year (2007-2011) database of meteorological profiles, collected from RAOBs carried out in Barajas Airport station (40.50º N, 3.57º W, 633 m.a.s.l), in Madrid, has been developed. Furthermore, a set of preprocessing and processing routines has been implemented, aiming to have a consistent database of meteorological profiles, discarding those ones having incomplete or unreal information. During this stage of the research, a novel method aimed to filter out those radiosoundings carried out during rainy conditions was proposed and validated under different meteorological conditions in Spain [22].

In view of collaborative works within the TeraSense project, where several groups are developing technology at 100 and 300 GHz, yearly statistics of atmospheric attenuation at both frequencies have been obtained using a total of 3332 RAOBs as input data. Several prediciton models have been tested in previous works [17,23] in order to calculate attenuation due to gases and clouds, being Liebe's [20] and Salonen's [22], respectively, the most accepted within the propagation community. The resulting statistics at the frequencies of interest, expressed in form of yearly Complementary Cumulative Distribution Functions (CCDFs), are shown in Figure 1a and 1b, respectively, where total attenuation is the combination of the effects of gases and clouds. The analysis of CCDFs show important differences on attenuation at both frequencies, caused by the strong influence of water vapor as frequency increases. While water vapor attenuation is the dominant factor at 300 GHz, gas and cloud attenuation present similar values at 100 GHz [23]. In general terms, differences are observed along the five years, particularly for time percentages below 10%, what can be attributed to the different occurrence of clouds in each year.

In addition, statistics provide us with useful information about the possibility of using radiometric technique in order to retrieve total attenuation values. This passive remote sensing technique could be used most of the time at 100 GHz due to the relatively low attenuation values observed, it means a non-saturation regime, with exception of rain conditions, where scattering influence can not be evaluated by a radiometer. At 300 GHz, this estimation would be quite difficult using radiometric techniques, except for the periods of the year with lowest water vapor concentration and absence of rain [23].

C. *Radiometric experiment at 99 GHz*

Following the above mentioned results concerning the implementation of a radiometer with the aim of developing propagation measurements under non-rainy conditions, a radiometric experiment was designed and implemented at UPM as a joint work with Radar and Microwave Group (GMR), also participating in the TeraSense project. The

instrument is an experimental prototype of a total-power radiometer working at 99 GHz, located at UPM facilities (see Figure 16), and implemented for the purpose of estimating total attenuation at this frequency along a 40º slant path. It corresponds to a non ad-hoc design, including commercial off-the-shelf (COTS) components and in-house circuits designed by GMR. Hardware implementation details, including useful layouts of its outdoor and indoor units, as well as calibration techniques developed for compensating the effects of gain variations and receiver noise temperature are extensively described in [24].

A short-term radiometric measurement campaign was performed from April 11th to 24th, 2012. During this period, sky conditions were predominantly characterized by the presence of clouds, being in some cases accompanied by precipitations. In addition, very stable and clear sky scenarios were also observed during a couple of days of the experiment. After processing of raw data at the output of the radiometer, attenuation values, A_T in (dB), are derived from sky brightness temperature measurements, which is the main parameter collected by radiometric instruments. Some relevant examples of time series of A_T, under the presence of clear sky and cloudy conditions, can be observed in Figures 17a and 17b, respectively. Very stable values of A_T are expected in absence of liquid water along the path under observation. Otherwise, in presence of clouds, measurements show a high sensitivity to the effects caused by liquid water. A comparative analysis included in [24], has shown that radiometric measurements are in agreement with attenuation estimations based on RAOBs data, collected during the period of time corresponding to the duration of the campaign, in combination with propagation models.

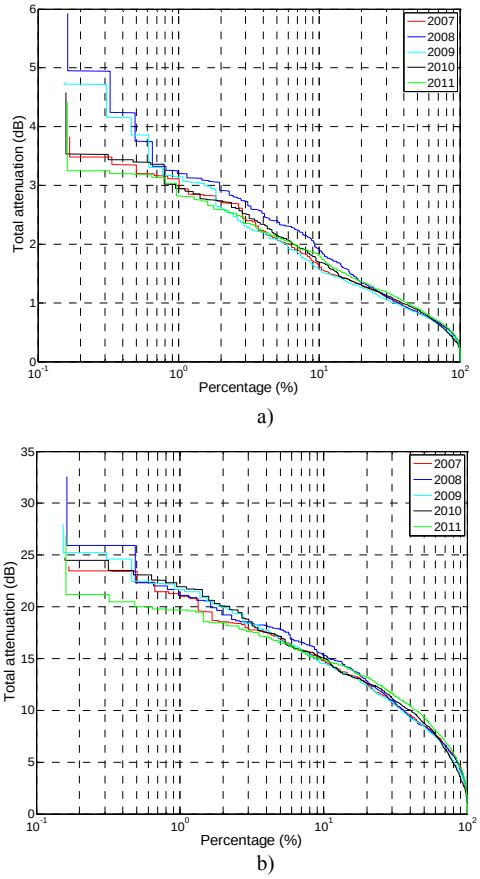

Fig. 15. Yearly CCDFs of atmospheric attenuation at a) 100 GHz and b) 300 GHz for Madrid/Barajas.

(a) (b)

Fig. 16. Radiometer at 99 GHz a) Outdoor unit, and b) General view during the campaign (left side).

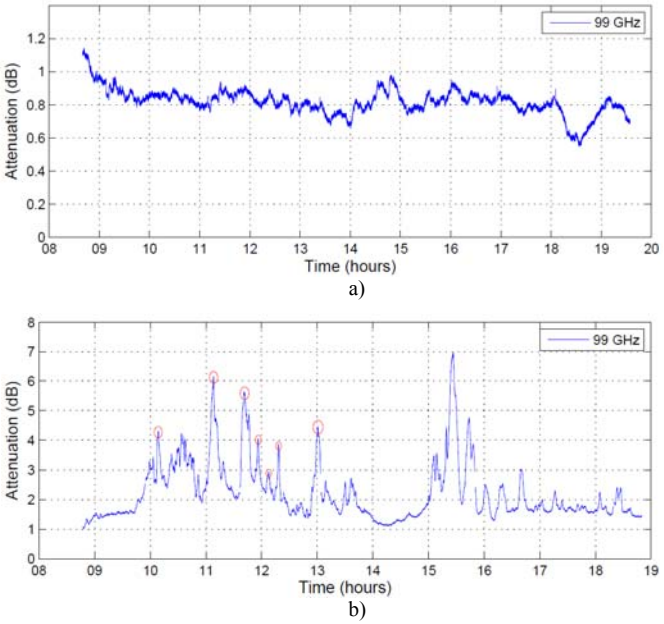

Fig. 17. Attenuation derived by radiometric measurements under a) clear sky (April 16th) and b) presence of clouds (April 20th).

V. Conclusions

The research within the antenna measurement domain has been focused in the implementation and test of antenna measurement set-ups at millimeter and sub-millimeter frequency bands, and on the other hand in the study of algorithms to improve the results of the antenna measurement systems and results. Also, algorithms have been designed for solving the time and memory constraints in the design of compact ranges at 100 or 300 GHz frequency bands.

From a general point of view, the research within the propagation domain was developed following two well differentiated and necessary stages. First, the propagation medium under non-rainy conditions was characterized using meteorological information. At this point, statistics from 5-years of RAOBs data, in addition to the exhaustive checking procedures and rain detection method implemented, provide a valuable reference tool on yearly levels of atmospheric attenuation caused by gases and clouds at 100 and 300 GHz in Madrid. Secondly, the use of a low-cost radiometer and single calibration techniques has shown promising results regarding the estimation of atmospheric attenuation using this technique. Additionally, to the best of our knowledge, this is

the first experiment of validation of using a radiometer around 100 GHz for propagation experiments in Spain.

ACKNOWLEDGEMENTS

The authors want to thank the TERASENSE (CSD2008-00068) project approved under the 2008 CONSOLIDER-INGENIO program.

REFERENCES

[1] A. Muñoz-Acevedo, M. Sierra-Castañer, J.L. Besada, "Antenna Measurement System at 300 GHz for the Terasense Project," *Proceedings of the 4th European Conference on Antennas and Propagation*, Barcelona April 2010.

[2] A. Muñoz-Acevedo, M. Sierra-Castañer, J.L. Besada, "Antenna Measurement System Operating at W and J Millimeter Wave Bands," *Proc. irmmwTHz conference*, Rome, 5th -10th September 2010.

[3] A. Munoz-Acevedo, M. Sierra-Castaner, "An Efficient Hybrid GO-PWS Algorithm to Analyze Conformal Serrated-Edge Reflectors for Millimeter-Wave Compact Range", IEEE Transactions on Antennas and Propagation, Volume: 60, Issue: 2, Part. 2 DOI: 10.1109/TAP.2011.2173100, Page(s): 1192 – 1197. February 2012

[4] P. Anderson and S. Sali, "New possibilities for phaseless microwave diagnostics-Part I: Error reduction techniques," Proc. Inst. Elect. Eng., vol. 132, pp. 291–298, Aug. 1985.

[5] S. F. Razavi and Y. Rahmat-Samii, "Phaseless planar near field measurements for scanned beams: Difficulties, a hybrid solution and measured results," in Proc. IEEE Antennas Propagation Society Int. Symp, vol. 9-14, 2006, pp. 429–432.

[6] G. Junkin, T. Huang, and J. Bennett, "Holographic testing of terahertz antennas," IEEE Trans. Antennas Propagat., vol. 48, no. 3, pp. 409 – 417,Mar. 2000.

[7] A. Tamminen, J. Ala-Laurinaho, and A. V. Räisänen, "Imaging with indirect holographic method at 310 GHz," in Proc. XXXI Finnish URSI convention on radio science and electromagnetics, 2008, pp. 31–32.

[8] Y. Alvarez, F. Las-Heras, and M. Pino, "Reconstruction of equivalent currents distribution over arbitrary three-dimensional surfaces based on integral equation algorithms," IEEE Transactions on Antennas and Propagation, vol. 55, no. 12, pp. 3460 –3468, Dec. 2007.

[9] Cebrián García González, Ana Arboleya Arboleya, Yuri Álvarez López, Jaime Laviada Martínez, Fernando Las-Heras Andrés, "Montaje de medidas para la reconstrucción de perfiles a 90 GHz", XXVII Simposium Nacional de la Unión Científica Internacional de Radio (URSI 2012), Elche, España, Sep. 2012.

[10] Ana Arboleya Arboleya, Cebrián García González, Yuri Álvarez López, Jaime Laviada Martínez, Fernando Las-Heras Andrés, "Millimeter and Submillimeter Wave Measurement System Implementation", XXVII Simposium Nacional de la Unión Científica Internacional de Radio (URSI 2012), 4págs en Actas, Elche, Sept. 2012.

[11] M. Sierra Castañer, A. Muñoz-Acevedo, F. Cano-Fácila, S. Burgos. Chapter 9: "Overview of novel post-processing techniques to reduce uncertainty in Antenna Measurements", pp. 179-204. INTECH. "Measurement System / Book 2". ISBN: 979-953-307-479-4. Year 2012

[12] F. Cano Facila, M. Sierra-Castaner. Methods for Noise Reduction in Far-Field Patterns Obtained from Cylindrical Near-Field Antenna Measurements. IEEE Transactions on Antennas and Propagation, Volume: 60, Issue: 12 Digital Object Identifier: 10.1109/TAP.2012.2208613 Publication Year: December-2012 , Page(s): 10

[13] Francisco José Cano-Fácila, Sergey Pivnenko, and Manuel Sierra-Castañer, "Reduction of Truncation Errors in Planar, Cylindrical, and Partial Spherical Near-Field Antenna Measurements", International Journal of Antennas and Propagation Volume 2012, Article ID 438727, 19 pages doi:10.1155/2012/438727, Year 2012

[14] Francisco José Cano-Fácila, Sara Burgos, Fernando Martín, and Manuel Sierra-Castañer, "New Reflection Suppression Method in Antenna Measurement Systems Based on Diagnostic Techniques", IEEE Transactions on Antennas and Propagation. DOI:10.1109/TAP.2010.2050426 Volume 59, Number 3, pp. 941-949, March 2011.

[15] Francisco Cano, Sara Burgos, Manuel Sierra-Castaner, "Novel method to improve the signal to noise ratio in far field results obtained from planar near field measurements", IEEE Antennas and Propagation Magazine, ISSN: 1045-9243, Vol. 53, Number 2, pp. 215-220, April 2011

[16] Muñoz-Acevedo, A.; Sierra-Castañer, M.; "Signal to Noise Ratio Maximization in Quiet Zone Acquisitions for Range Assessment at Sub-millimeter Wavelengths," Radioengineering, Vol. 21, no.2, June 2012

[17] G. Siles, J. Riera, and P. García-del-Pino, "Considerations on cloud attenuation at 100 and 300 GHz for propagation measurements within the TeraSense project," in Antennas and Propagation (EuCAP), Proceedings of the 5th European Conference on, 2011.

[18] J. Garcia-Rubia, J. Riera, P. García-del-Pino, and A. Benarroch, "Attenuation Measurements and Propagation Modeling in the W-Band," *Antennas and Propagation, IEEE Transactions on*, 2013. In Press.

[19] H. J. Liebe et al. "Propagation modeling of moist air and suspended water/ice particles at frequencies below 1000 GHz". *AGARD 52nd Specialists Meeting of the Electromagnetic Wave Propagation Panel*, Palma de Mallorca, Spain; 1993.

[20] P. W. Rosenkranz, "Water vapor continuum absorption: A comparison of measurements and models" *Radio Science*, vol. 33, no. 4, pp. 919–928, 1998.

[21] E. Salonen and S. Uppala, "New prediction method of cloud attenuation", *Electronics Letters*, vol. 27, pp. 1106-1108, 1991.

[22] G. Siles, J. Riera, P. García-del-Pino, and J. Romeu, "Atmospheric propagation at 100 and 300 GHz: Assessment of a method to identify rainy conditions during radiosoundings," *Progress In Electromagnetics Research*, vol. 130, pp. 257–279, 2012.

[23] G. A. Siles, J. M. Riera and P. García-del-Pino, "On the Use of Radiometric Measurements to Estimate Atmospheric Attenuation at 100 and 300 GHz", *Journal of Infrared, Millimeter and Terahertz Waves*, vol. 32, no. 4, pp. 528-540, Apr. 2011.

[24] G. Siles, J. Riera, P. Garcia-del Pino, B. Mencia-Oliva, and J. Grajal, "Estimation of Atmospheric Attenuation at 99 GHz Using a Total Power Radiometer," in Antennas and Propagation (EUCAP), Proceedings of the 7th European Conference on, Goteborg, Sweden, 2013.